DOI 10.1007/s11003-024-00765-y
Materials Science, Vol. 59, No. 2, September, 2023 (Ukrainian Original Vol. 59, No. 2, March–April, 2023)

QUANTITATIVE MODEL FOR THE PREDICTION OF THE CORROSION RATE OF COLD-ROLLED 316L STEEL

A. Dittes,[1,2] T. Mehner,[1] S. Friedrich,[3] B. Awiszus,[3] and T. Lampke [1]

The austenitic stainless steel 316L is used for numerous components due to its excellent corrosion resistance. However, forming of components influences the microstructure and can thus change the corrosion resistance of the steel. In this context, the corrosion rate of the steel 316L is determined for the case of uniform corrosion of various cold-rolled conditions by ageing tests in 0.5 M H_2SO_4. The microstrain, the martensite fraction, and the residual stress state are quantified using X-ray diffraction. The surface roughness is measured by laser scanning microscopy. Three different model equations are derived by means of multiple regression to predict the corrosion rate as a function of the specimen properties. The analysis shows that a particularly simple model equation, which predicts the corrosion rate only via the plastic strain, shows insufficiently large deviations from the experimentally determined corrosion rates. However, a low divergence to the experimental results with a mean deviation of less than 4% is achieved by using a model equation that takes microstructural parameters and the surface ratio into account. Within this model equation, an increased corrosion rate is achieved with higher microstrain and residual compressive stress of the austenite phase as well as a higher surface-area ratio. A higher fraction of martensite is found to lower the corrosion rate.

Keywords: corrosion, modeling, cold-forming, microstructure, austenitic stainless steel, martensitic transformation.

Introduction

Austenitic stainless steels like 304 and 316 steels are used in numerous components in chemical-plant engineering, food-processing industry, medical technology, heat exchangers, and as bipolar plates for fuel cells due to their high corrosion resistance. For bipolar plate manufacturing, various studies report a relationship between the forming production process and the resulting corrosion properties of the components [1–3]. However, these publications usually neglect the microstructural changes in the components caused by the forming process or only qualitatively observe the change of a selected parameter. The non-uniform forming is associated with significant changes in the microstructure and consequently local variations for formed components, which in turn may impact the local corrosion behavior.

Forming processes like rolling often introduce preferential grain orientations. In this context, study [4] on the potential-free corrosion of polished and solution-annealed, fully austenitic 316L specimens in 0.5 M $H_2SO_4 - LiCl$ solution have shown the corrosion rate increase with the following scaling {001} < {101} < {111} of the grain orientations.

[1] Materials and Surface Engineering Group, Institute of Materials Science and Engineering, Chemnitz University of Technology, Germany.
[2] Corresponding author; e-mail: axel.dittes@mb.tu_chemnitz.de
[3] Virtual Production Engineering Group, Institute for Machine Tools and Productions Processes, Chemnitz University of Technology, Germany.

Published in Fizyko-Khimichna Mekhanika Materialiv, Vol. 59, No. 2, pp. 88–97, March–April, 2023. Original article submitted December 22, 2022.

Furthermore, deformation-induced martensite is frequently reported for cold-worked 304 and 316 steels [5–9]. Cold-working-induced α′-martensite and deformation bands in 304L steel are reported in [5]. They are electrochemically less noble than the surrounding austenitic matrix. Thus, local gradients of the corrosion potential cause microgalvanic elements that increase the local corrosion rate [5].

Other studies address the effect of mechanical or residual stresses, defects, and martensite on the passive layer. Electrochemical studies performed on 304L steel under constant elastic tensile stress showed that the diffusivity for species in the passive layer increases with mechanical loading, indicating increased corrosion susceptibility [10]. This is confirmed by Mott–Schottky analyses on moderately cold-rolled 304 steel (with near-surface tensile residual stress), whereas the diffusivity of the passive layer is lowered for a severely cold-rolled condition, which has strong compressive residual stresses in the specimen surface due to pronounced formation of martensite [6]. In addition, another investigation showed that an accumulation of defects, e.g. dislocations, in the austenite due to rolling causes microstrain (MS) that increases the diffusivity of the passive layer [11].

The studies mentioned above indicate that forming processes alter various microstructural properties of stainless steels, which have an impact on the passive film and the corrosion behavior. However, the studies often target a single microstructural parameter and examine small and localized effects, so that no transfer to complex forming processes or components is possible. Quantitative models are required which describe the relationships between the forming process, the microstructure evolution and the resulting corrosion rate with sufficient accuracy. The integration of such models into finite-element-method (FEM) simulations would allow for a better design of forming processes with regard to the local and global corrosion resistance of the produced components. In this context, this paper presents a quantitative multiple-regression model for cold-rolled sheets of 316L steel that links the near-surface microstructure caused by cold rolling to the corrosion rate for the simple case of uniform corrosion.

Materials and Methods

Material and Specimen Production by Cold Rolling. The material used in this study was a 2 mm thick metal sheet of 316L steel (EN 1.4044, supplier: Marcegaglia Specialities). In the initial state, the material was treated by solution-annealing at 1050°C and quenching. The material composition was determined by glow-discharge optical emission spectroscopy (mass%): 0.03 C; 17.31 Cr; 10.55 Ni; 2.38 Mo; 1.14 Mn; 0.3 Si; 0.02 P; < 0.01 S; 0.46 Cu; 0.22 Co; 0.06 V; 0.01 Nb; Fe – bal.

Samples (size 80×40×2 mm) were cut from the 316L sheet using a water jet and then processed by rolling at ambient temperature. A dual-reversing rolling mill with a roller diameter of 236 mm and a constant rolling speed of 3.77 rpm was applied. A total of 14 sample conditions were produced by different rolling sequences (Table 1). Specimens with a size of 30 mm in rolling direction and 20 mm in transverse direction were extracted from the center of the rolled sheet by water-jet cutting and investigated with regard to the microstructure and corrosion behavior. This area provides a homogenous microstructure and residual stress distribution, as evaluated by preliminary tests. The plastic strain (PS) of the variously rolled specimens was calculated using Simufact V2021.1 simulation software by applying a close-to-reality cold-rolling model and averaging elements of the specimen surface in the center area.

Specimen Characterization. *Surface roughness*. The surface roughness of rolled and cut specimens (20×30 mm) was studied by laser scanning microscopy (LSM) with a VK-X200 microscope (Keyence) equipped with a laser withUU a wave length λ = 408 nm. An area of 5000×5600 μm was recorded with ×20 magnification. For the recorded data, two areas (4800×450 μm and 450×4800 μm in size) were evaluated with the software VK Analyzer (Keyence). With respect to the corrosion rate, the surface-area ratio (SAR) was

determined as a ratio of the real surface area (A_{real}) to the nominal surface area (A_{nom}), and the mean value of the two areas was used as the characteristic parameter for the multiple regression analysis.

Table 1
Rolling Sequences Used for Specimen Production and Corresponding Plastic Strain

Rolling sequence	Rolling passes [mm]	Final thickness δ [mm]	PS	Multiple regression *
As-received	2, solution-annealed	2	0	TS
Sequence 2-1.5	2 → 1.5	1.5	0.32	TS
	2 → 1.5 → 1.3	1.3	0.50	VS
	2 → 1.5 → 1.3 → 1.1	1.1	0.70	TS
	2 → 1.5 → 1.3 → 1.1 → 0.9	0.9	0.94	VS
	2 → 1.5 → 1.3 → 1.1 → 0.9 → 0.7	0.7	1.24	TS
Sequence 2-1.7	2 → 1.7	1.7	0.17	TS
	2 → 1.7 →1.5	1.5	0.32	VS
	2 → 1.7 → 1.5 → 1.3	1.3	0.49	TS
	2 → 1.7 → 1.5 → 1.3 → 1.1	1.1	0.69	TS
	2 → 1.7 → 1.5 → 1.3 → 1.1 → 0.9	0.9	0.93	TS
	2 → 1.7 → 1.5 → 1.3 → 1.1 → 0.9 → 0.7	0.7	1.23	TS
Sequence 2-1.8	2 → 1.8	1.8	0.09	TS
	2 → 1.8 → 1.5	1.5	0.31	TS

* The kind of used samples for the multiple regression is indicated as follows: training samples (TS) and validation samples (VS).

Microstrain, phase composition, and residual-stress state. X-ray diffraction (XRD) was performed using a diffractometer D8 Discover (Bruker) with Co K_α -radiation (point focus, irradiated area of approximately 1.2 mm in diameter) and an energy-sensitive 1D detector LYNXEYE XE-T. Diffraction diagrams were measured in the diffraction-angle (2θ) range 20–130° (step size 0.03°, step time 7.5 s/step) and evaluated by line-profile analyses (software Topas, Bruker) in order to determine the phase fractions (α-martensite, austenite) and their MS. The {311} peak of the austenite phase was used for residual-stress each in the positive and negative tilt direction with nine tilt angles ψ that were equally spaced on the $\sin^2\psi$ axis from 0.0 to 0.8 ($\sin^2\psi$ method). The evaluation was done in the software Leptos (Bruker) with a biaxial model with shear stresses and the corresponding elastic constants of Young modulus $E^{\{311\}}$ = 175 GPa and Poisson ratio $\nu^{\{311\}}$ = 0.31 [12]. XRD is averaging over an information depth of approximately 15 μm for the investigated steel 316L.

Corrosion experiments. Corrosion experiments were conducted for rolled and cut specimens (30×20 mm) and six specimens were tested for each rolling condition. Without further preparation, the specimens were ultrasonically degreased in ethanol and fully immersed for 20 days in 500 ml of 0.5 M H_2SO_4 at 30°C within a closed beaker with constant mechanical stirring at 150 rpm. Samples of 10 ml each were taken from the electrolyte (1 h; 3 h; 5 h; 1 day; 2 days; 3 days; 6 days; 10 days; 15 days; and 20 days). The concentrations of the main alloying elements: iron, chromium, and nickel were determined at $\lambda_{Fe} = 238.204$ nm, $\lambda_{Cr} = 267.716$ nm, or $\lambda_{Ni} = 221.648$ nm by inductively coupled plasma with optical emission spectroscopy (ICP-OES) using an Optima 8300 spectrometer (Perkin Elmer). The time-dependent corrosion rate (C_{corr}) was calculated from the sum of the mass of dissolved iron, nickel, and chromium ions m_{tot}, the overall surface area A_{nom}, the mass density ρ of 316L steel (8.0 g/cm³) and the corrosion exposure time t using the equation:

$$C_{corr}(t) = \frac{m_{tot}(t)}{A_{nom}} \times \rho \times t .$$

Prediction of Microstructure Corrosion Models by Multiple Regression Analysis. Correlations between the microstructure, residual stresses, roughness and the corrosion rate were determined by multiple regression using the analysis of variance (ANOVA) with a square model including interactions between the parameters (optimization algorithm: least squares). The modeling was done on eleven training samples (TS). Three samples were used as validation samples (VS) to test the validity of the model (Table 1). For both the TS and VS, the absolute and average deviations between the measured and modeled values were used in the parameter-selection process while maintaining a low number of degrees of freedom.

Results and Discussion

Effect of Cold Rolling on the Near-Surface Specimen Properties. The surface roughness was investigated for different rolled specimen conditions and evaluated in terms of the SAR (Fig. 1). The differences between the individual specimen conditions are at most approximately 20%. The initial, 2 mm thick specimen condition has by far the highest SAR. As the thickness is reduced by successive rolling passes, the SAR of the specimens decreases because the less rough surface profiles of the rollers are imprinted into the specimens. For thicknesses of 1.3 mm and lower, roughly a constant value of about 1.15 is achieved, whereby slightly higher SAR values are observed for the rolling sequence 2-1.5 compared to the rolling sequence 2-1.7.

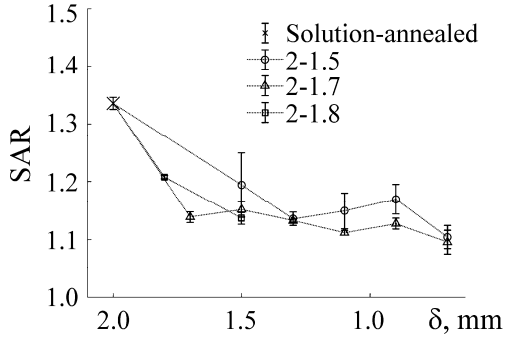

Fig. 1. Evolution of the surface-area ratio of the rolled 316L specimens determined by LSM. Designations in Table 1.

The MS is a measure of the density of short-range defects such as voids and dislocations. The as-received specimen condition has a very low MS, which can be explained by the prior solution-annealing treatment. With an increasing thickness reduction by cold-rolling, the MS strongly increases the dislocation density (Fig. 2*a*). A comparable tendency for 316L steel was reported in [8]. For the different rolling sequences, no pronounced difference in the evolution of the MS with rolling passes is apparent. Along with an increasing dislocation density in 316L samples, the dislocations typically arrange and form deformation twins. Deformation-induced martensite predominantly nucleates at the boundary between the twin and the austenite matrix as reported in [9].

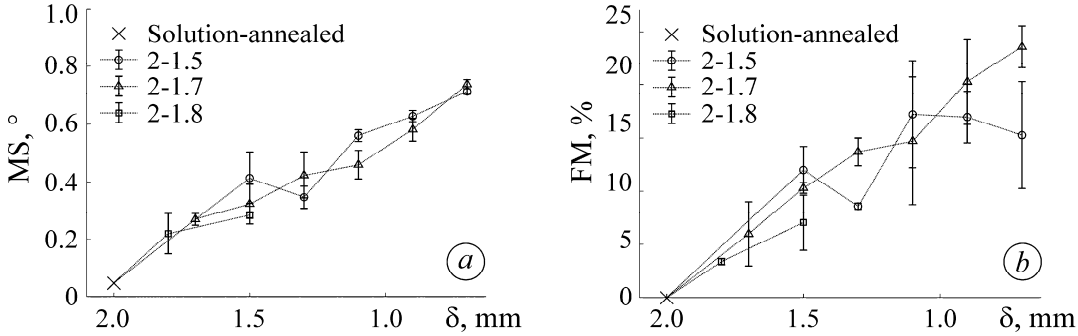

Fig. 2. Microstrain of (*a*) austenite and fraction of (*b*) α′-martensite determined by XRD. Designations in Table 1.

The α′-martensite fraction of the differently rolled specimens was determined by XRD (Fig. 2*b*). Note that no ε-martensite was recorded in the underlying diffraction diagrams. The initial specimen condition (2 mm thickness) shows no martensite as no cold-working was applied. In general, an increasing fraction of martensite (FM) is observed with increasing thickness reduction by rolling, whereby the rate at which martensite is formed decreases progressively when compared to the introduced PS. This tendency is also typically reported by others for 316L steel [13]. For specimens with a thickness of 1.5 mm, the FM differs depending on the applied rolling sequence. Here, the FM of the sequence 2-1.5 is higher than that of sequence 2-1.7, which is again higher than the sequence 2-1.8. The opposite trend in the FM is observed for the sequences 2-1.5 and 2-1.7 for severely rolled specimen conditions for specimens with thicknesses of 0.9–0.7 mm.

Furthermore, the evolution of the 1st and the 2nd principal stresses of the austenite was determined by XRD (Fig. 3). With the specimen thickness reduction by cold rolling, strong compressive residual stresses are introduced into the surface. The compressive residual stresses can be explained by the formation of α′-martensite, which increases in volume relative to the parent austenite grains [6]. Hence, the compressive residual stresses of the specimen conditions are well-aligned to the FM (Fig. 2*b*). The most pronounced compressive stress is observed at a specimen thickness of 0.9 mm. A further rolling pass to 0.7 mm lowers the compressive stresses of both rolling sequences 2-1.5 and 2-1.7. This effect is stronger for the sequence 2-1.5 and can be explained by the different evolution of the FM of both rolling sequences at the rolling pass 0.9 mm → 0.7 mm. While the FM is increased for the sequence 2-1.7, it is slightly lowered for the sequence 2-1.5. The slight decrease of the compressive residual stress, which is observed for the sequence 2-1.7 even though the FM rises, is explained as follows. The rolling process itself typically introduces tensile residual stresses to the rolled specimen, but those are superimposed by the compressive residual stresses caused by the formed martensite [6]. In this context, the author of [14] reported increasing tensile residual stresses in severe cold rolling of 316L steel, where there was no martensite.

The time-dependent evolution of the corrosion rates of three selected sample conditions is shown in Fig. 4*a*. At the beginning of the corrosion experiments (1 h), a particularly strong metal dissolution takes place. For all tested specimen conditions, a rapid decrease in the corrosion rate over time is observed that tends towards a

time-infinite asymptote C_{corr_∞}. Note, that the initial particularly intensive mass dissolution in the electrolytes is caused by an additional corrosion process (e.g. rapid corrosion of a few very corrosion-susceptible grains), which quickly decays. For this reason, the correlation of corrosion rate and electrolyte exposure time was fitted by a decaying exponential function using only data of 3 days and more exposure time (Fig. 4*a*). The characteristic parameter C_{corr_∞} was extracted (Fig. 4*b*) and was used for the subsequent modeling. The solution-annealed initial specimen condition has the lowest C_{corr_∞}.

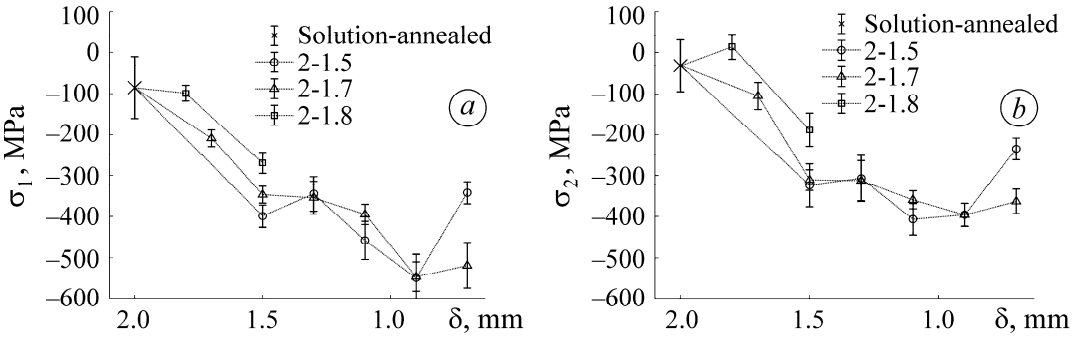

Fig. 3. Principal stresses (*a*) σ_1 and (*b*) σ_2 of rolled 316L specimens determined by XRD. Designations in Table 1.

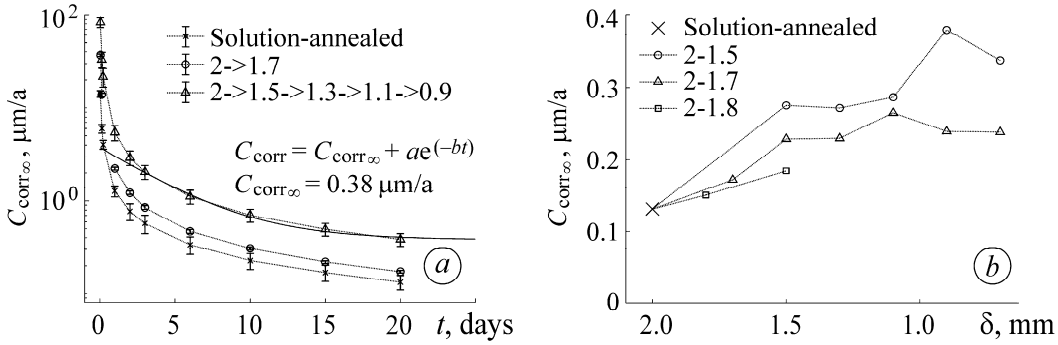

Fig. 4. Determination of the asymptote of the corrosion rate for (*a*) a selected specimen condition and (*b*) the corresponding time-infinite corrosion rates of the rolled 316L specimens. Designations in Table 1.

With increasing thickness reduction of the rolled specimens, a higher C_{corr_∞} value is observed. This tendency is comparable to other studies [8], in which an increasing corrosion susceptibility for rolled 316L steel using potentiodynamic polarization experiments, was reported. The evolution of C_{corr_∞} for different thicknesses depends on the rolling sequence (Fig. 4*b*). For all specimen conditions of the sequence 2-1.5 with a particularly large first rolling pass, a higher C_{corr_∞} was determined than for the sequence 2-1.7 with a medium first rolling pass. The lowest C_{corr_∞} was observed for the sequence 2-1.8 that had a small first rolling pass. For the sequences 2-1.5 and 2-1.7, C_{corr_∞} appears to approach a saturation value for high thickness reductions, but the difference in the level of C_{corr_∞} is still present.

Multiple Regression for the Determination of Microstructure–Corrosion Relationships. For the data presented, three model equations (MoEq1, MoEq2, and MoEq3) were established using multiple regression and ANOVA to correlate the cold-rolling induced properties of the specimens to the corrosion rate (Table 2). MoEq1 is motivated by the objective of integrating the prediction of the local corrosion rate into FEM simulations that are performed during the design of the component forming processes, using input variables that are easily accessible. Therefore, MoEq1 contains only the PS as an input parameter, which is typically accessed by such simulations.

The objective of MoEq2 is to account for the microstructure that is altered by the rolling process because, as outlined in the introduction, it has a significant effect on the corrosion behavior. The MS and residual stress of the austenite and the FM were included. MoEq3 additionally considers the size of the actual surface area as an input parameter. It can be assumed that the surface area accessible to the electrolyte significantly influences the corrosion rate.

MoEq1 is based on three summands, one of which is a constant value that depicts the corrosion rate of the solution-annealed initial specimen condition. The second summand is linearly coupled with the PS. It increases the predicted corrosion rate. The third summand is proportional to PS^2 and it reduces the predicted corrosion rate. Hence, it is particularly important for large PS values. By this, the saturation effect of the PS on the corrosion rate is included in the MoEq1. However, the high p-value (13.9%) of PS^2 indicates that the significance of this parameter is statistically not well-assured. The MoEq1 offers a rough estimate of the corrosion rate, but the prediction accuracy is insufficient. This is apparent by the comparison to the experimentally determined corrosion rates (Table 2), which shows average deviations of 11% for the TS and 15% for the VS and even high maximum deviations of up to 26% for certain specimen conditions.

In comparison, MoEq2 and MoEq3 require more measurements and methods in order to determine the required microstructural parameters. However, the corrosion rates predicted by MoEq2 and MoEq3 agree much better with the experimental results. They provide average deviations of less than 6 and 4% respectively (Table 2). Furthermore, the maximum deviations for individual specimen conditions are less than 13.3% or 12.5% and thus are significantly lower compared to MoEq1. MoEq2 and MoEq3 both require a constant and three summands that contain, in different combinations, the MS, the residual stress of austenite, and the FM. The associated p-values are negligibly small, which indicates the significance of these parameters. Note that the applicability of these MoEqs is strictly limited to compressive residual stresses as no TS with sufficient tensile residual stress were available. The SAR, which is additionally included in MoEq3, is associated with an increasing corrosion rate. This explains the improved prediction accuracy compared to MoEq2.

For MoEqs 2 and 3, the MS and residual stress of the austenite increase the calculated corrosion rate, whereas the FM reduces the corrosion rate. The multiplicative coupling of the residual stress and MS parameters in MoEq2 indicates that the superposition of the long- and short-range mechanical stress fields particularly increases the corrosion rate. In MoEq3, the multiplicative coupling of the MS and SAR parameters indicates that a large real surface with a high MS disproportionately increases the corrosion rate. This could be caused by the higher number of electrolyte-exposed faces of those defect-rich faster-corroding grains when A_{real} is larger.

The identified decrease of the corrosion rate with higher FM is contrary to another study [5], which describes martensite as electrochemically less noble than austenite and that thus suggests microgalvanic elements that lead to accelerated martensite dissolution. The relationships found in the presented MoEqs (when both austenite and martensite are present) can be explained as follows: for the underlying mechanism of hydrogen-type acid corrosion, from a kinetic point of view, the cathodic reaction (hydrogen evolution) is the corrosion-rate determining reaction, i.e., it is significantly slower than the anodic metal dissolution. As a consequence, higher corrosion rates are achieved when the cathodic area (austenite) is large.

Table 2
Model Equations for the Prediction of C_{corr_∞} and Deviations Between Model Equation and Experimentally Derived C_{corr_∞} for TS and VSE

MoEq1 ($R^2 = 0.690$): $C_{\mathrm{corr}_\infty}\left(\frac{\mu\mathrm{m}}{\mathrm{a}}\right) = 0.1353 + 0.2795 \times \mathrm{PS} - 0.1319 \times (\mathrm{PS})^2$

Parameter	*p*-value [%]
PS	< 3.1
PS²	< 13.9

Sample group	Average deviation [%]	Maximum deviation [%]
TS group	10.6	23
VS group	14.9	25.8

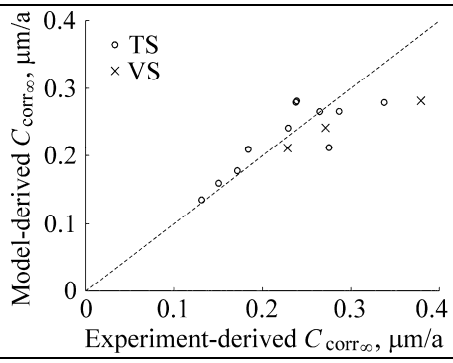

MoEq2 ($R^2 = 0.966$): $C_{\mathrm{corr}_\infty}\left(\frac{\mu\mathrm{m}}{\mathrm{a}}\right) = 0.0987 + 0.2916 \times \mathrm{MS}(^\circ) - 0.00093 \times \sigma_2 \times \mathrm{MS}(\mathrm{MPa} \times ^\circ) - 0.00059 \times \mathrm{FM}^2(\%^2)$

Parameter	*p*-value [%]
MS	< 0.1
$\sigma_2 \times$ MS	< 0.1
FM^2	< 0.1

Sample group	Average deviation [%]	Maximum deviation [%]
TS group	4.6	13.2
VS group	6.0	9.6

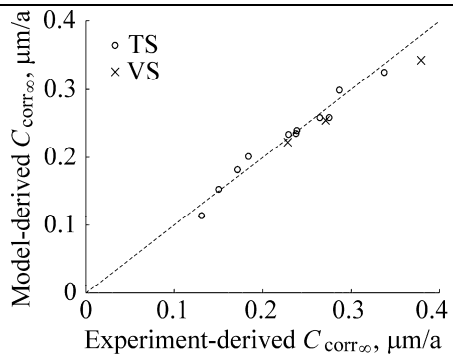

MoEq3 ($R^2 = 0.971$): $C_{\mathrm{corr}_\infty}\left(\frac{\mu\mathrm{m}}{\mathrm{a}}\right) = 0.0709 - 0.00049 \times \sigma_2(\mathrm{MPa}) - 0.0197 \times \mathrm{FM}(\%) + 0.5648 \times \mathrm{SAR} \times \mathrm{MS}(^\circ)$

Parameter	*p*-value [%]
σ_2	< 0.1
FM	< 0.1
SAR×MS	< 0.1

Sample group	Average deviation [%]	Maximum deviation [%]
TS group	3.9	12.5
VS group	3.7	8.8

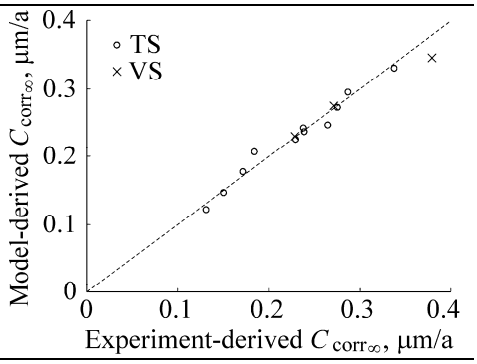

Note: MoEq is a model equation, SAR is $A_{\mathrm{real}}/A_{\mathrm{nom}}$. The given *p*-value marks the error probability that the observed correlation is purely caused by statistical deviations (i.e. that the null hypothesis is more plausible).

With an increasing martensite content (anodic area), the ratio of the anodic and cathodic areas shifts to a larger anode proportion so that the total corrosion rate is reduced. Note that the FM determined by XRD is an average over a depth of about 15 μm and does not include any local information regarding the depth. Thus, it is unclear if the actual FM directly at the surface is significantly higher, which would decrease the cathodic area even more. Due to the deformation-induced formation of martensite during the rolling process, high martensite contents occur in the same sample conditions in which the austenitic matrix is also more plastically deformed so that there is a correlation between the parameters of MS and FM (Fig. 2). The strong plastic deformation of austenite introduces a high defect density (i.e. high MS values), which causes the austenite to become electrochemically less noble [5]. In consequence, the potential difference between austenite and martensite becomes smaller and thus the driving force of the microgalvanic element is reduced with higher PS and thus FM. As a result, the high FM in the samples with higher thickness reductions has a mitigating effect on the corrosion rate.

The outcome of both MoEqs is that the corrosion rate is increased with more pronounced residual compressive stress. This seems to be in contrast to the theory that the diffusivity of the passive layer and thus the corrosion susceptibility is lowered by compressive stresses as the interatomic spacing is reduced. This is assumed, for example in [6], who reported about Mott–Schottky analyses on cold-rolled 304 steel. They found a lower diffusivity of the passive layer for a highly rolled specimen condition with strong compressive stresses due to a high fraction of strain-induced martensite in comparison to a less rolled condition that show tensile stress [6]. In this context, although no conclusion on the corrosion susceptibility was made, it was shown [15] that the passive-film thickness, which is formed on the compressive-stress-affected surface of U-shaped bend specimens made of 302 steel, is higher compared to the opposite surface that shows tensile stress [15]. Furthermore, another study [16] investigated the passive layer properties of ground as well as polished 304L steel specimens with different compressive residual stresses [16]. They showed that the ground condition, which had by far the strongest compressive residual stresses, exhibited the thinnest passive layer with the highest diffusivity.

CONCLUSIONS

In the present study, the microstructure, surface roughness, and the corrosion rate of 316L steel samples were investigated for different cold-rolled conditions. The relationship between microstructural properties and the resulting corrosion rate for uniform corrosion in 0.5 M H_2SO_4 was evaluated in different model equations. Although PS can be determined easily, its sole consideration in a model proved to provide insufficient prediction accuracy. The best prediction of the corrosion rate with an average deviation to experimental data of less than 4% is achieved using a model equation that includes the residual stress and the MS of austenite, the fraction of deformation-induced martensite, and the SAR. For those parameters, the corrosion rate is increased by the residual stress, the MS and the SAR, whereas the FM is lowering the corrosion rate. With respect to the underlying experimental data, the applicability of the model equation is limited to cold-worked specimens with only compressive residual stresses and to the mechanism of uniform corrosion with a small material removal.

The model equations can be integrated into FEM simulations of the cold-rolling processes. This allows for the prediction and optimization of rolling-process routes of components regarding corrosion properties. Further work should address the transferability of the model equations established in this study to other forming processes. An improved accuracy of the model equation can be achieved by adding the influence of texture and possible near-surface heterogeneities of the microstructure.

Acknowledgements. The authors acknowledge the financial support for this research provided by the German Research Foundation (DFG) granted within funding number 428159001 (projects AW 6/40-1 and ME 5420/1-1).

REFERENCES

1. F. Dundar, E. Dur, S. Mahabunphachai, and M. Koç, "Corrosion resistance characteristics of stamped and hydroformed proton exchange membrane fuel cell metallic bipolar plates," *J. of Power Sources*, **195**, Is. 11, 3546–3552 (2010); https://doi.org/10.1016/j.jpowsour.2009.12.040
2. M. F. Peker, Ö. N. Cora, and M. Koç, "Surface topography evolution during long-run micro-stamping of bipolar plates (BPPS) and effects on corrosion and contact resistance characteristics," in: *Proc. of the ASME 2012 Int. Mech. Eng., Congress & Exposition IMECE-2012* (2012), pp. 3035–3039; https://doi.org/10.1115/IMECE2012-85461
3. M. F. Peker, Ö. N. Cora, and M. Koç, "Investigations on the variation of corrosion and contact resistance characteristics of metallic bipolar plates manufactured under long-run conditions," *Int. J. of Hydrogen Energy*, **36**, Is. 23, 15427–15436 (2011); https://doi.org/10.1016/j.ijhydene.2011.08.067
4. S. Dong, X. Chen, E. C. La Plante, M. Gussev, J. Leonard, and G. Sant, "Elucidating the grain-orientation dependent corrosion rates of austenitic stainless steels," *Mat. and Des.*, **191**, art. no. 108583 (2020); https://doi.org/10.1016/j.matdes.2020.108583
5. X. Chen, M. Gussev, M. Balonis, M. Bauchy, and S. Gaurav, "Emergence of micro-galvanic corrosion in plastically deformed austenitic stainless steels," *Mat. and Des.*, **203**, art. no. 109614 (2021); https://doi.org/10.1016/j.matdes.2021.109614
6. G. Monrrabal, A. Bautista, S. Guzman, C. Gutirrez, and F. Velasco, "Influence of cold working induced martensite on the electrochemical behavior of AISI 304 stainless steel surfaces," *J. of Mat. Res. and Techn.*, **8**, Is. 1, 1335–1346 (2019); https://doi.org/10.1016/j.jmrt.2018.10.004
7. S. Tanhaei, K. Gheisari, and S. R. Alavi Zaree, "Effect of cold rolling on the microstructural, magnetic, mechanical and corrosion properties of AISi 316L austenitic stainless steel," *Int. J. of Minerals, Metallurgy and Materials*, **25**, Is. 6, 630–639 (2018); https://doi.org/10.1007/s12613-018-1610-y
8. V. Tandon, A. P. Patik, and R. C. Rathod, "Correlation of martensite content and dislocation density of cold worked 316L on defect densities of passivating film in acidic environment," *Mat. Res. Express.*, **5**, Is. 8, art. no. 086515 (2018); https://doi.org/10.1088/2053-1591/aacee9
9. N. Nakada, H. Ito, Y. Matsuoka, T. Tsuchiyama, and S. Takaki, "Deformation-induced martensitic transformation behavior in cold-rolled and cold-drawn type 316 stainless steel," *Acta Materialia*, **58**, Is. 3, 895–903 (2010); https://doi.org/10.1016/j.actamat.2009.10.004
10. D. Sidane, O. Devos, M. Puiggali, M. Touzet, B. Tribollet, and V. Vivier, "Electrochemical characterization of a mechanically stressed passive layer," *Electrochemistry Communications*, **13**, Is. 12, 1361–1364 (2011); https://doi.org/10.1016/j.elecom.2011.08.010
11. S. K. Pradhan, P. Bhuyan, L. R. Bairi, and S. Mandal, "Comprehending the role of individual microstructural features on electrochemical response and passive film behavior in type 304 austenitic stainless steel," *Corros. Sci.*, **180**, art. no. 109187 (2021); https://doi.org/10.1016/j.corsci.2020.109187
12. B. Eigenmann, and E. Macherauch, "X-ray investigation of stress states in materials [Röntgenographische untersuchung von spannungszuständen in werkstoffen: Teil III]," *Materialwissenschaft und Werkstofftechnik*, **27**, Is. 9, 426–437 (1996); https://doi.org/10.1002/mawe.19960270907
13. M. Naghizadeh, and H. Mirzadeh, "Modeling the kinetics of deformation-induced martensitic transformation in AISI 316 metastable austenitic stainless steel," *Vacuum*, **157**, 243–248 (2018); https://doi.org/10.1016/j.vacuum.2018.08.066
14. B. Ravi Kumar, B. Mahato, and R. Singh, "Influence of cold-worked structure on electrochemical properties of austenitic stainless steels," *Metallurgical and Materials Transactions A: Physical Metallurgy and Materials Science*, **38A**, Is. 9, 2085–2094 (2007); https://doi.org/10.1007/s11661-007-9224-4
15. F. Navaï, "Effects of tensile and compressive stresses on the passive layers formed on a type 302 stainless steel in a normal sulphuric acid bath," *J. of Mat. Sci.*, **30**, Is. 5, 1166–1172 (1995); https://doi.org/10.1007/BF00356115
16. K. Jaffré, B. Ter-Ovanessian, H. Abe, N. Mary, B. Normand, and Y. Watanabe, "Effect of mechanical surface treatments on the surface state and passive behavior of 304L stainless steel," *Metals*, **11**, Is. 1, art. no. 135 (2021); https://doi.org/10.3390/met11010135